Spectroscopy of ^{110}Sn via the high-resolution ^{112}Sn$(p, t)^{110}$Sn reaction

P. Guazzoni and L. Zetta
Dipartimento di Fisica dell'Università, and Istituto Nazionale di Fisica Nucleare, Via Celoria 16, I-20133 Milano, Italy

A. Covello and A. Gargano
Dipartimento di Scienze Fisiche, Università di Napoli Federico II, and Istituto Nazionale di Fisica Nucleare, Complesso Universitario di Monte S. Angelo, Via Cintia, I-80126 Napoli, Italy

B. F. Bayman
School of Physics and Astronomy, University of Minnesota, Minneapolis, Minnesota, USA

G. Graw, R. Hertenberger, and H.-F. Wirth
Sektion Physik der Universität München, D-85748 Garching, Germany

M. Jaskola
Soltan Institute for Nuclear Studies, Warsaw, Poland
(Received 1 August 2006; published 14 November 2006)

The ^{112}Sn$(p, t)^{110}$Sn reaction was studied in a high-resolution experiment at an incident proton energy of 26 MeV. Angular distributions for 27 transitions to levels of ^{110}Sn up to an excitation energy of ∼4.3 MeV were measured. A distorted-wave Born approximation (DWBA) analysis of experimental angular distributions using conventional Woods-Saxon potentials were done, allowing either the confirmation of previous spin and parity values or the assignment of new spin and parity to a large number of ^{110}Sn states. A shell-model study was performed using an effective interaction derived from the CD-Bonn nucleon-nucleon potential. The energy spectra are calculated and compared with experiment, whereas the theoretical two-nucleon spectroscopic amplitudes, evaluated in a truncated seniority space, are used in the microscopic DWBA calculation of some cross-section angular distributions.

DOI: 10.1103/PhysRevC.74.054605 PACS number(s): 25.40.Hs, 21.10.Hw, 21.60.Cs, 27.60.+j

I. INTRODUCTION

Many experimental and theoretical investigations have been carried out for the nuclei near the $Z = 50$ closed shell. Due to the existence of a large number of stable isotopes, the tin isotopes are particularly suited for studying the evolution of nuclear structure when the 50–82 neutron shell is filled. Both odd and even tin isotopes have been investigated. Much information has been collected for the heavier isotopes, but the properties of the lighter isotopes are less well known. To extend the systematics to the lighter tin isotopes, we studied ^{114}Sn [1] using the (p, t) reaction in high-resolution measurements. In the present work, we extend this program to include ^{110}Sn. Two-neutron transfer reactions are very sensitive to pairing correlations in the overlap between initial and final states. Therefore, as a specific probe of this type of correlations, the (p, t) reactions play a fundamental role in the study of the structure of low-spin states of nuclei.

In the tin isotope region, five active neutron orbitals $0g_{7/2}$, $1d_{5/2}$, $1d_{3/2}$, $2s_{1/2}$, and $0h_{11/2}$, contribute to the state structure. To study the interplay and the mixing of configurations associated with these orbitals, we require a large amount of experimental data concerning both low-spin and high-spin states. The linked use of different techniques, such as γ-ray spectroscopy (with both selective and nonselective reactions), β decay, and transfer reactions, allows us to achieve this aim.

The nucleus ^{110}Sn has been studied from β^+ decay of ^{110}Sb [2]. γ-ray spectroscopy measurements led to the construction of a decay scheme, including 36 transitions among 18 low-lying states of ^{110}Sn. Spins and parities of the states involved in the decay were deduced.

High-spin neutron quasiparticle excitations in ^{110}Sn nucleus were investigated using the ^{108}Cd$(\alpha, 2n\gamma)^{110}$Sn reaction [3]; spin assignments to levels of ^{110}Sn were based on angular distributions only. Linear-polarization measurements were not carried out.

Nanosecond isomers of ^{110}Sn were investigated using ^{110}Cd$(^3$He$,3n)^{110}$Sn $(5.2 \pm 0.8$ ns) and ^{104}Pd$(^{12}$C$,2n\alpha)^{110}$Sn $(5.6 \pm 0.4$ ns) at 29 and 63 MeV bombarding energies, respectively. A partial level scheme of ^{110}Sn was deduced [4].

In a search for collective behavior at high spin and high excitation energy, some levels of ^{110}Sn have been identified using the reactions ^{94}Mo$(^{19}$F$,p2n\gamma)^{110}$Sn at 83 MeV, together with a γ-ray multiplicity filter [5]. A deformed intruder band in the high-spin region of ^{110}Sn was identified by Harada *et al.* [6] using the ^{98}Mo$(^{16}$O$,4n\gamma)^{110}$Sn reaction.

The mechanism of these fusion-evaporation reactions induced by heavy ions is very selective for high spin states, and preferably populates states with high alignment, whereas transfer reactions are better at characterizing low-spin states. Therefore, the two kinds of reactions complement each other both in their degree of selecting particular states and in their spin and energy range.

TABLE I. Isotopic composition of the ^{112}Sn target

Isotope	112	114	115	116	117	118	119	120	122	124
Percentage	98.9	1.0	<0.05	<0.05	<0.02	<0.02	<0.02	<0.02	<0.02	<0.02

Fleming *et al.* [7] performed a (p, t) study on several even Sn isotopes at an incident proton energy of 20 MeV, with an energy resolution of 25 keV. In the ^{112}Sn$(p, t)^{110}$Sn reaction, only the transitions to the ground state and first excited 2^+ state were observed, due to the low proton incident energy and the severe negative Q value. A ^{112}Sn$(p, t)^{110}$Sn experiment with a resolution of 14 keV was carried out by Blankert [8] at a proton energy of 27.5 MeV. Levels up to ∼4.5 MeV of excitation energy were identified and L values determined up to ∼3.3 MeV, but these results were never published. For this reason we performed a new study of the ^{112}Sn$(p, t)^{110}$Sn reaction, using a high-resolution experiment to characterize the low-spin states of ^{110}Sn.

Cross-section angular distributions of 25 (p, t) transitions, including two doublets, to the final states of ^{110}Sn up to an excitation energy of 4.317 MeV were obtained. This also allows determination of the angular-momentum transfers to 27 levels and the assignment of spin and parity values to 27 levels.

In connection with the experimental work, we have carried out DWBA microscopic calculations of cross-section angular distributions for the ground state and some excited states of ^{110}Sn, using two neutron spectroscopic amplitudes obtained from a shell-model study of the 12- and 10-neutron systems outside the $N = 50$ major neutron shell, in ^{112}Sn target nucleus and ^{110}Sn residual nucleus, respectively. The shell-model calculations of the motion of these neutrons have been carried out within the framework of the seniority scheme using a realistic effective interaction derived from the CD-Bonn nucleon-nucleon potential [9]. The model space has been truncated to states with seniority less than or equal to 4 to reduce the numerical work required by a complete-basis diagonalization.

A full shell-model study of both positive- and negative-parity spectra of ^{110}Sn has been also performed. It is worth noting that preliminary results of the present study were published in Ref. [10].

The outline of the article is as follows. In Sec. II the experimental method and analyzing procedure are described. Section III is devoted to an outline of our shell-model calculations and to the comparison with experiment of the theoretical spectra and the cross-section angular distributions. Section IV contains a summary of our conclusions.

II. EXPERIMENTAL METHOD AND ANALYZING PROCEDURE

A. Experiment

The (p, t) experiment was carried out using the 26-MeV proton beam delivered by the HVEC MP tandem accelerator of the MLL (Maier-Leibnitz Laboratory of LMU Munich and TU Munich) laboratory. The beam current intensity ranged from 200 to 350 nA to avoid target heating. The ^{112}Sn target, whose isotopic enrichment is given in Table I, had a thickness of 102 μg/cm^2 on a carbon backing of 13 μg/cm^2. Thanks to the higher isotopic enrichment of our target, compared to the one used by Blankert [8] (isotopic enrichment of ^{112}Sn target amounts to 83.5%), we measured triton spectra free of contributions from the different tin isotopes.

The reaction products have been analyzed with a Q3D magnetic spectrograph [11] and detected in its focal plane at 10 angles between 6° and 57.5° relative to the beam axis in two different magnetic field settings to reach an excitation energy of 4317 keV in the ^{110}Sn residual nucleus. The spectrograph has a solid angle acceptance of 2.98 msr for $\theta = 6°$ and 11.04 msr for $\theta \geqslant 10°$.

The 1.8-m-long focal plane detector [12] for light ions consists of an array of single-wire proportional detectors with an additional readout structure, followed by a rest energy plastic scintillator detector. This device provides position determination, ΔE-E identification, and focal plane reconstruction. The excellent energetic characteristics of the accelerator, the spectrograph, and the detector enable us to perform high-resolution measurements of the triton spectra with a resolution of about 8 keV full width at half maximum.

The incident proton beam is stopped in a Faraday cup, the integrated current allowing measurements of absolute differential cross sections. The uncertainties regarding the target thickness, solid angle, collected charge, and background subtraction at high excitation energies give a systematic error of ∼15%. The dead time was negligible.

The triton spectra were analyzed with the Autofit shape-fitting code [13], using the shape of the triton peak at 2545 keV as a reference. The areas and centroids of the triton peaks were determined.

The high resolving power of the spectrograph, the reduced background, the large solid angle, and the spectrum energy resolution allowed measurement of the cross sections of rather weakly populated levels. For example, the level at 2753 keV assigned as $(6)^+$ in the adopted level scheme [14], which was identified up to now only in ^{94}Mo(^{19}F,$p2n\gamma$) [5], ^{98}Mo(^{16}O,$4n\gamma$) [6], and ^{108}Cd(α, $2n\gamma$) [3] studies, is populated in the present (p, t) reaction with a maximum cross section of a few μb/sr.

The energy calibration of the spectra was performed by using the adopted excitation energies of eight levels determined in γ-decay [14] measurements and identified also in our (p, t) experiment. The correlation between the measured channels and the excitation energies was established with a polynomial of rank 4. The parameters of the polynomial were fixed in the energy range from 0 up to 4317 keV by imposing the reproduction of the eight adopted energies. The achieved uncertainties on our quoted energies are estimated at 3 keV.

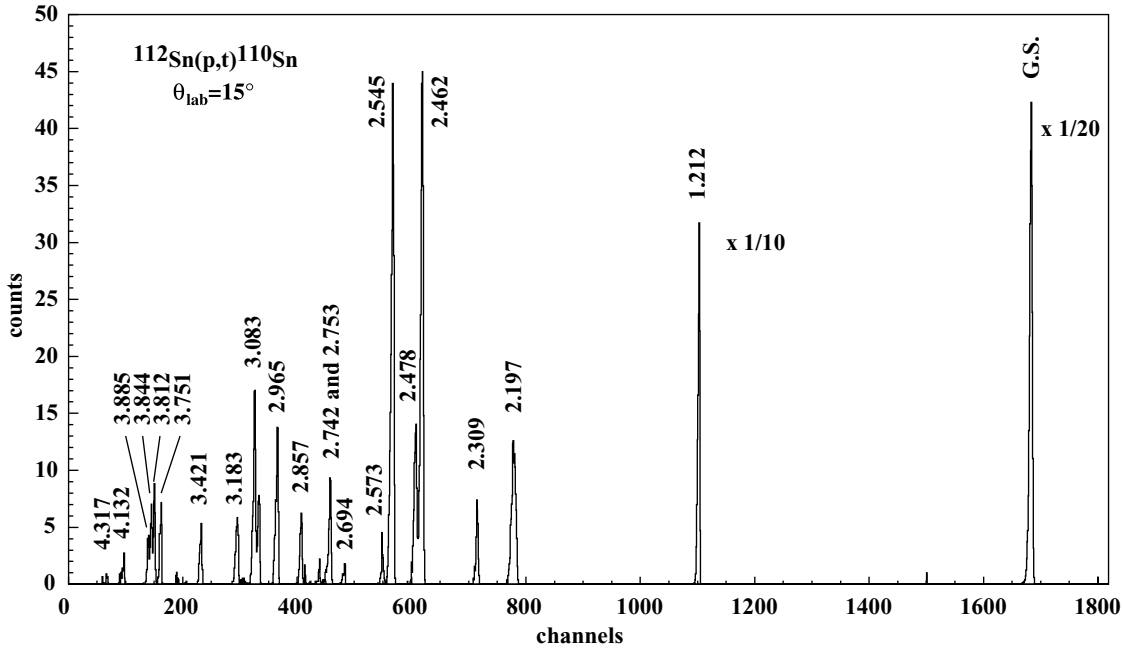

FIG. 1. Position spectrum of tritons measured at $\theta = 15^\circ$. Some levels are labeled with their excitation energy in MeV.

Figure 1 shows an example of the measured spectra. In this spectrum at $\theta = 15^\circ$, the excitation energies of the most prominent peaks are indicated.

We have studied 27 (p, t) transitions to the final states of ^{110}Sn up to $E_x = 4317$ keV, of which 9 are identified for the first time and their spin and parity assigned by the distorted-wave Born approximation (DWBA) analysis reported in the next subsection.

Table II reports the spectroscopic information on ^{110}Sn, deduced from the present experiment and compared with information available in the literature [14]. The integrated experimental cross sections, estimated with a systematic error of 15%, are also reported in the last column of Table II, together with the statistical errors.

B. Cluster DWBA analysis

Two-neutron transfer reactions, such as (p, t), have been extensively used as spectroscopic tools for studying even-even nuclei. In the case of a 0^+ initial state, and assuming that the neutrons are transferred in a relative $L = 0$ state with total spin $S = 0$, a one-step transfer process populates only natural-parity states in the residual nucleus. Then the J^π of the final states are unambiguously inferred by L-transfer identification $[J_f = L, \pi_f = (-1)^L]$.

For the transitions populating the ^{110}Sn states, a DWBA analysis has been performed, assuming a semimicroscopic dineutron cluster pickup mechanism. Our DWBA analysis of ^{110}Sn transitions is along the same lines of that performed in the case of ^{114}Sn [1], with the basic assumption that the relative motion of the transferred spin-singlet neutron pair has zero orbital angular momentum and no radial nodes. The center-of-mass wave function of the transferred neutron pair is then described by a single-particle wave function whose angular momentum equals the total angular momentum L of the transferred pair.

The radial dependence of the center-of-mass wave function is obtained by solving the radial Schroedinger equation for the dineutron, requiring that the number of radial nodes N be given by the conservation law for three-dimensional harmonic oscillator quanta:

$$Q = 2N + L = \sum_{i=1}^{2} (2n_i + \ell_i),$$

where n_i and l_i are the quantum numbers of the individual shell-model states that form the transferred pair. The calculated angular distributions are determined mainly by L, and are only slightly affected if N changes by one. The shapes of the angular distributions depend very little on the detailed microscopic shell-model components of the transferred dineutron cluster. For these reasons, the DWBA calculations are a valuable tool in the use of the observed angular distributions to extract the transferred angular momenta L. However, the detailed shell-model structure of the cluster, i.e., the n_i and l_i values of the component of the dineutron cluster and the relative phases with which these components appear in the cluster, is important to determine the *magnitude* of the transfer cross section.

In Sec. III, we present calculations of the shell-model spectroscopic amplitudes and their use together with the DWBA transfer amplitudes to obtain relative cross sections for different states in ^{110}Sn.

The DWBA calculations have been carried out in finite-range approximation, using the computer code TWOFNR [15] and a proton-dineutron interaction potential of Gaussian form $V(r_{p2n}) = V_0 \exp[-(r_{p2n}/\xi)^2]$ with $\xi = 2$ fm. The parameters for the proton entrance channel are deduced from a systematic survey of elastic scattering by Perey [16] and for the triton

TABLE II. Column 1 gives the adopted energies of the ^{110}Sn levels (in upright type) and the experimental uncertainties (in italics) as reported in Ref. [14]; column 2 gives the adopted spins and parities [14]; columns 3 and 4 the energies, spins and parities observed in the present work; column 5 gives the integrated cross sections from 6° to 57.5°. Our quoted energies are estimated to have an uncertainty of ±3 keV. In column 5 absolute cross sections, estimated with a systematic error of ±15%, are reported together with the statistical errors.

^{110}Sn level scheme					
Adopted			Present experiment		
E_{exc}(keV)		J^π	E_{exc} (MeV)	J^π	$\sigma_{int}(\mu b)$
0.0		0^+	0.0	0^+	1309 ± 14
1211.88	*15*	2^+	1.212	2^+	198 ± 6
2120.92	*25*	(2)			
2196.92	*15*	4^+	2.197	4^+	61 ± 2
2302		0^+	2.309	0^+	12 ± 1
2455.5	*3*	4^+			
2459		(3^-)			
			2.462 D	$4^+ + 3^-$	88 ± 2
2477.7	*6*	6^+	2.478	6^+	44 ± 1
2545.5	*5*	2^+	2.545	2^+	36 ± 1
2579		0^+	2.573	0^+	7.1 ± 0.5
2694.4	*5*	4^+	2.694	4^+	11 ± 1
2745		0^+	2.742	0^+	18 ± 1
2753.8	*6*	$(6)^+$	2.753	6^+	6.5 ± 0.5
2802.3	*6*				
2821.3	*4*	(2,3,4,5)			
2833.4	*4*	2^+			
			2.857	2^+	7.7 ± 0.5
2914.7	*10*	2^+			
2948.1	*3*	$(2^+, 3^+, 4^+, 5^+)$			
2964.8	*6*		2.965	2^+	14 ± 1
2977.0	*5*				
2983		4^+			
2997		(2^+)			
			3.059	4^+	36 ± 1
3060		0^+			
			3.083	2^+	16 ± 1
3153		2^+			
3182.8	*7*	$(2^+, 3^+, 4^+, 5^+)$			
			3.183	0^+	17 ± 1
3222.5	*4*	$(2^+, 3^+, 4^+, 5^+)$			
3252		4^+			
3320		2^+			
3357		5^-			
			3.421	2^+	6.3 ± 0.5
3446.6	*6*	$(2^+, 3^+, 4^+, 5^+)$			
3540.4	*7*	(2,3,4)	3.540	4^+	3.3 ± 0.4
			3.609	4^+	5.5 ± 0.5
3629.7	*4*	$(2^+, 3^+, 4^+, 5^+)$			
3687.0	*6*	$(7)^-$			
			3.751	2^+	5.3 ± 0.4
3765.2	*9*	$(8)^-$			
3807					
			3.812	2^+	11 ± 1
3812.5	*6*	$(8)^+$			
			3.844	5^-	14 ± 1
3884.9	*7*	$(2^+, 3^+, 4^+, 5^+)$	3.885	3^-	2.6 ± 0.3
3933.1	*9*	$(9)^-$			

TABLE II. *(Continued.)*

^{110}Sn level scheme					
Adopted			Present experiment		
E_{exc}(keV)		J^π	E_{exc} (Mev)	J^π	$\sigma_{int}(\mu b)$
3971					
			4.132 D	$3^- + 5^-$	5.1 ± 0.4
4158					
4316.8	*7*	(10)	4.317	4^+	4.1 ± 0.4

exit channel by Fleming *et al*. [7] and were adjusted slightly to improve the agreement with the experimental angular distributions. Alternative proton [17] and triton [18] potentials have been tried, using the ground-state transition as a test case, but they give poorer fits. In Table III the optical model parameters for the proton and triton continuum wave functions, and the geometrical parameters used for evaluating the bound-state wave functions of the transferred dineutron cluster, are summarized. The optical model parameters reported in Table III have been also used to analyze the angular distributions of ^{122}Sn$(p,t)^{120}$Sn measured at 20 [7] and 26 MeV [19,20], ^{116}Sn$(p,t)^{114}$Sn [1] at 26 MeV and ^{123}Sb$(p,t)^{121}$Sb at 26 MeV [21], giving good agreement between experimental results and DWBA calculations. The good agreement suggests that multistep processes, which are not taken into account in the present DWBA calculations, are small in this region of masses and at this bombarding energy.

The comparison between experimental and calculated shapes of the angular distributions allows the assignment of transferred angular momentum values. The experimental data and the results of the calculations for different L transfers are compared in Figs. 2–5 and generally good agreement is found. DWBA curves are quite different for different L transfers, and the clear structure of the angular distribution is rather well described by the DWBA calculations. In Fig. 5 the angular distributions of the unresolved doublets at 2.462 and 4.132 MeV are compared with the theoretical calculations. For the two doublets the percentage of the two different L contributions have been determined imposing the lowest value of χ^2.

C. Spin and parity assignment

As shown in Table II, we have made spin and parity assignments for all the observed levels. In particular, nine levels have been observed for the first time and identified in J^π. With respect to the adopted levels (NDS) [14], 10 assignments have been confirmed and four ambiguities removed. Two unresolved doublets have been observed, giving one confirmation, one removed ambiguity, and 2 new assignments.

In the following, we propose assignments for those levels observed in the present experiment that were not previously observed or that are reported in the adopted level scheme [14] with uncertain, or without, J^π assignment. Assignments are also proposed for the two unresolved doublets.

2.462 MeV. The NDS [14] report two levels with energies 2455.5 and 2459 keV with $J^\pi = 4^+$ and (3^-) respectively. The first one was identified in the ^{98}Mo(^{16}O,4$n\gamma$) [6], and ^{108}Cd(α, 2$n\gamma$) [3] reactions and, together with the second one, in the ^{112}Sn$(p,t)^{110}$Sn reaction [8] as members of a close-lying doublet. The positive parity of the first one is attributed on the basis of β^+-decay study [2]. J^π of the two levels are assigned on the basis of the L transfer from the (p,t) reaction. Our measured angular distribution is well reproduced by assuming that this transition corresponds to an unresolved doublet of one level with $J^\pi = 4^+$ ($L = 4$ transfer 30%) and another level with $J^\pi = 3^-$ ($L = 3$ transfer 70%).

2.753 MeV. The adopted level scheme [14] reports a level at 2753.8 keV identified in ^{94}Mo(^{19}F,$p2n\gamma$) [5], ^{98}Mo(^{16}O,4$n\gamma$) [6], and ^{108}Cd(α, 2$n\gamma$) [3] reactions with tentative $(6)^+$ spin assignment. In the present work, the angular distribution is quite well reproduced by assuming $L = 6$ transfer. The present assignment is $J^\pi = 6^+$.

2.857 MeV. At this energy, the adopted level scheme [14] gives no level. The observed level, weakly excited in our experiment, is consistent with an attribution of 2^+.

2.965 MeV. In Ref. [14], a level is given at an energy of 2964.8 keV, inferred from the ^{108}Cd(α, 2$n\gamma$) [3] reaction without spin and parity attribution. In our measurement this level is reasonably populated, and the angular distribution is fairly well reproduced by an $L = 2$ transfer. The present attribution is $J^\pi = 2^+$.

TABLE III. The Woods-Saxon optical-model parameters for the incident proton, the outgoing triton, and the geometrical parameters for the bound state of the transferred dineutron cluster.

	V_r (MeV)	r_r (fm)	a_r (fm)	W_v (MeV)	r_v (fm)	a_v (fm)	W_d (MeV)	r_d (fm)	a_d (fm)	V_{so} (MeV)	r_{so} (fm)	a_{so} (fm)	r_c (fm)
p	50.0	1.25	0.65				10.0	1.30	0.60	3.00	1.25	0.70	1.25
t	176.0	1.14	0.72	18.0	1.61	0.82				8.00	1.10	0.80	1.30
B.S.		1.30	0.50										

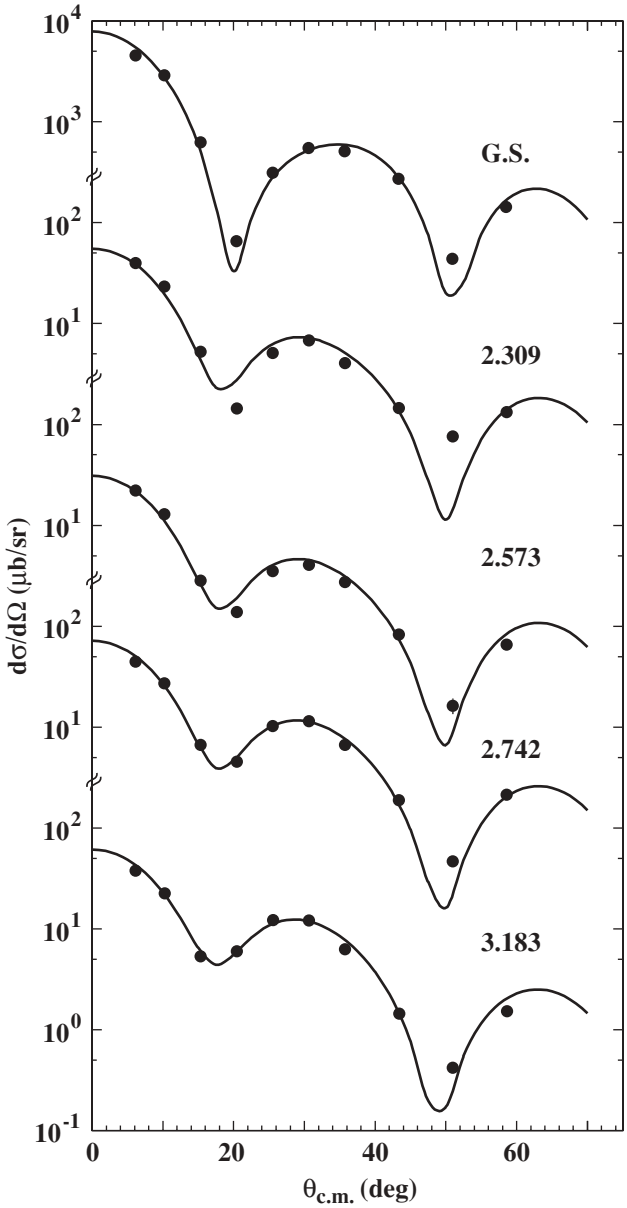

FIG. 2. Differential cross sections for the excitation of 0^+ states by the ^{112}Sn$(p, t)^{110}$Sn reaction. The dots represent the experimental data, the solid lines the theoretical estimates obtained with semimicroscopic DWBA calculations. The energies attributed to the observed levels are those given in the present work.

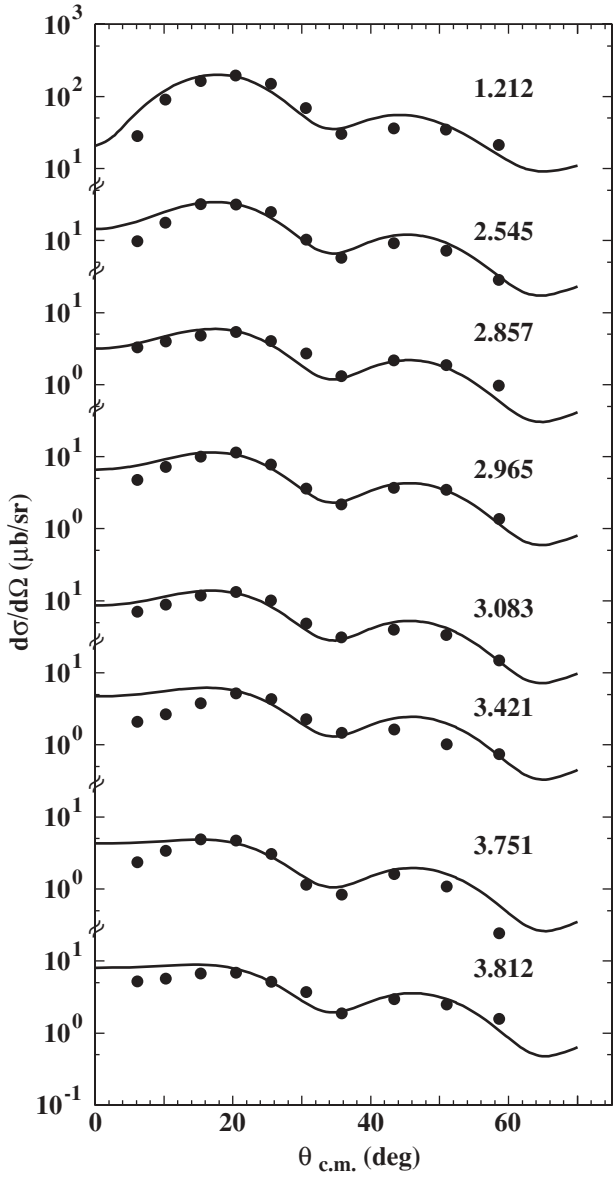

FIG. 3. Differential cross sections for the excitation of 2^+ states by the ^{112}Sn$(p, t)^{110}$Sn reaction. The dots represent the experimental data, the solid lines the theoretical estimates obtained with semimicroscopic DWBA calculations. The energies attributed to the observed levels are those given in the present work.

3.059 MeV. The adopted level scheme [14] gives a 0^+ level at 3060 keV, on the basis of the (p, t) reaction measured by Blankert [8]. This attribution is incompatible with our findings because it would imply the typical $L = 0$ pattern in the differential cross section angular distribution of a very steeply rising cross section at very small reaction angles and sharp minimum at the detector angle of about 20°. This is in conflict with the typical $L = 4$ transfer shape of the angular distribution that we observed. The J^π value assigned in the present work is 4^+.

3.083 MeV. No level is given at this energy by the adopted level scheme [14]. The angular distribution is quite accurately reproduced by considering an $L = 2$ transfer. The present assignment is $J^\pi = 2^+$.

3.183 MeV. The adopted level scheme [14] reports a level at an energy of 3182.8 keV with tentative spin and parity assignments $(2^+, 3^+, 4^+, 5^+)$, deduced from ^{110}Sb β^+ decay [2]. In our measurement, the angular distribution displays a typical $L = 0$ shape, well reproduced by the DWBA calculation. We assign $J^\pi = 0^+$ to this level, which most probably does not coincide with the level reported in NDS [14] at 3182.8 keV.

3.421 MeV. At this energy no level is reported in the adopted level scheme [14]. In our experiment this level is weakly

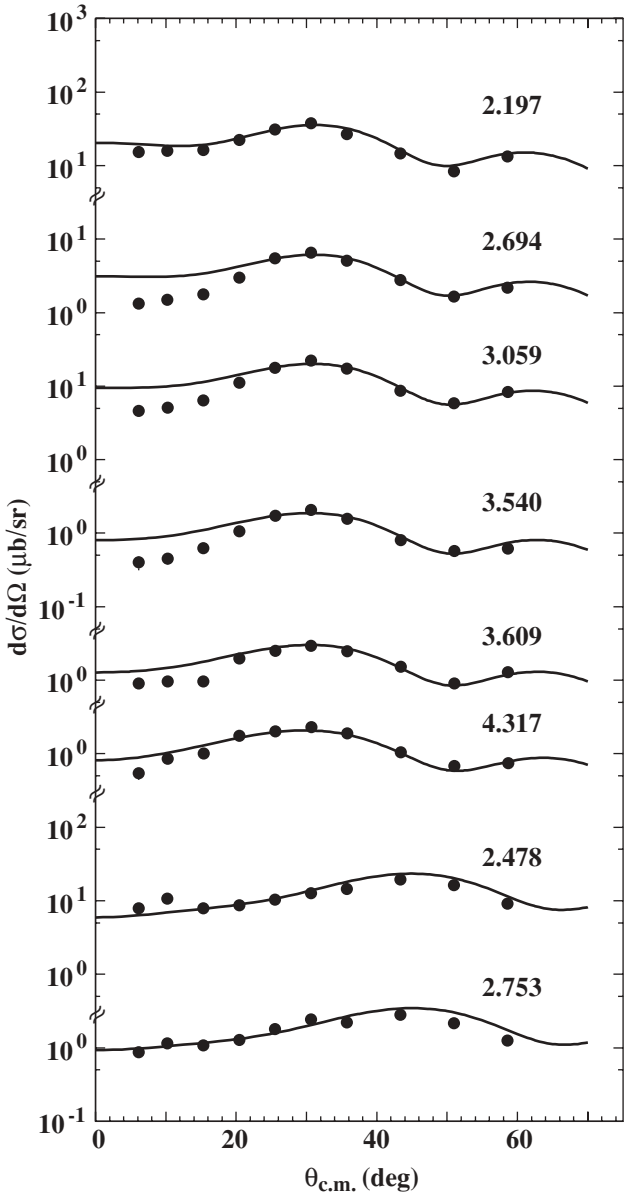

FIG. 4. Differential cross sections for the excitation of the six observed 4^+ and the two observed 6^+ states by the ^{112}Sn$(p,t)^{110}$Sn reaction. The dots represent the experimental data, the solid lines the theoretical estimates obtained with semimicroscopic DWBA calculations. The energies attributed to the observed levels are those given in the present work.

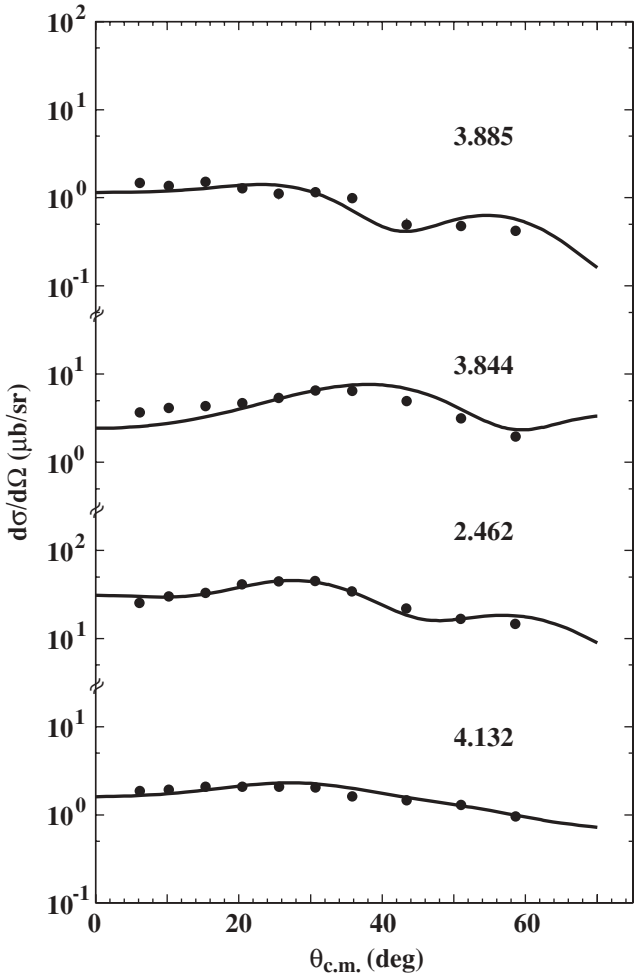

FIG. 5. Differential cross sections for the excitation of 3^- 3.885-MeV and 5^- 3.844-MeV states, and the two doublets at 2.462 MeV and 4.132 MeV by the ^{112}Sn$(p,t)^{110}$Sn reaction. The dots represent the experimental data and the solid lines the theoretical estimates obtained with semimicroscopic DWBA calculations. The energies attributed to the observed levels are those given in the present work.

populated. The measured angular distribution is consistent with an attribution of $J^\pi = 2^+$.

3.540 MeV. In Ref. [14] a level is given at an energy of 3540.4 keV, derived from ^{110}Sb β^+ decay [2] with tentative spin attribution (2,3,4). In our (p,t) measurement the level at 3.540 MeV is quite weakly populated and an $L = 4$ transfer reasonably reproduces the angular distribution. The present assignment is $J^\pi = 4^+$.

3.609 MeV, 3.751 MeV, 3.844 MeV. At these energies no levels are given in the adopted level scheme [14]. Accurate reproductions of the angular distributions are obtained by assuming the values $J^\pi = 4^+$, $J^\pi = 2^+$, and $J^\pi = 5^-$, respectively.

3.812 MeV. The adopted level scheme [14] reports a level (without spin and parity attribution) at 3807 keV, observed in the (p,t) reaction [8]. Van Poelgest *et al.* [3] report a level at 3812.5 keV with tentative spin and parity (8^+). In the present experiment, the 3.812-MeV level is weakly populated and the angular distribution is consistent with an attribution $J^\pi = 2^+$. This level probably coincides with the level reported in NDS [14] at $E_{ex} = 3807$ keV.

3.885 MeV. In Ref. [14], a level is listed at 3884.9 keV with tentative J^π attribution $(2^+, 3^+, 4^+, 5^+)$ from the ^{110}Sb β^+ decay [2]. In our measurement, the angular distribution of the tritons weakly populating the level at 3.885 MeV is reasonably well reproduced by an $L = 3$ transfer. The present attribution is therefore $J^\pi = 3^-$.

4.132 MeV. At this energy no level is given in the adopted level scheme [14]. In our study this level is weakly populated

and we accurately reproduce the differential cross section by considering an unresolved doublet with $J^\pi = 3^-$ (50%) and $J^\pi = 5^-$ (50%).

4.317 MeV. A level at 4316.8 keV from the ^{108}Cd$(\alpha, 2n\gamma)$ experiment by Van Poelgest *et al.* [3] is reported on the adopted level scheme [14] with tentative spin assignment (10). A satisfactory reproduction of the angular distribution is obtained by assuming the values $J^\pi = 4^+$ for spin and parity.

III. MICROSCOPIC CALCULATIONS

A. Shell-model calculations and comparison with the experimental energy spectrum

We assume that ^{100}Sn is a closed core and let the valence neutrons occupy the five levels $0g_{7/2}$, $1d_{5/2}$, $1d_{3/2}$, $2s_{1/2}$, and $0h_{11/2}$ of the 50–82 shell.

As input to our shell-model calculation we need the neutron single-particle (SP) energies as well as the neutron-neutron matrix elements of the effective interaction, which, as mentioned in the Introduction, have been derived from the CD-Bonn nucleon-nucleon potential [9]. This potential, as all modern ones, contains a strong short-range repulsion that prevents its direct use in nuclear structure calculations. To overcome this difficulty we construct a renormalized low-momentum potential, $V_{\text{low-k}}$, that preserves the physics of the original nucleon-nucleon potential up to a certain cutoff momentum Λ [22]. In particular, the scattering phase shifts and the deuteron binding energy calculated from the bare potential are reproduced by the corresponding $V_{\text{low-k}}$. The latter is a smooth potential that is well suited to replace the bare potential in many-body calculations and has proven to be an advantageous alternative to the traditional Brueckner G matrix.

Once the $V_{\text{low-k}}$ is calculated, it may be used to derive the two-body effective interaction. This has been performed within the framework of the $\hat{Q}$-box plus folded-diagram method [23]. In our calculation of the $\hat{Q}$-box we include all diagrams up to second order in $V_{\text{low-k}}$, which has been constructed with a cutoff momentum $\Lambda = 2.1\,\text{fm}^{-1}$ according to the criterion discussed in Ref. [22]. These diagrams have been calculated within a harmonic-oscillator basis inserting intermediate states composed of particle and hole states restricted to the two major shells above and below the $N = Z = 50$ Fermi surface. The oscillator parameter used is $\hbar\omega = 8.5$ MeV. The effective interaction is then obtained by summing to the $\hat{Q}$-box the folded diagrams to all orders. This has been performed by using the Lee-Suzuki iterative method [24]. A description of the derivation of the effective interaction, including references, can be found in Ref. [25].

Note that the interaction obtained by this procedure represents the effective interaction between two-valence neutrons outside the doubly closed ^{100}Sn and may be not completely adequate for systems with several valence particles, as is the case of ^{110}Sn. In the present study, however, we have not attempted to modify the effective interaction derived as described above.

As regards the neutron SP energies, they cannot be taken from experiment, because no spectroscopic data are yet available for ^{101}Sn. Here we have adopted, with the only exception of $\epsilon_{h_{11/2}}$, the values previously determined by an analysis of the low-energy spectra of light odd Sn isotopes in Ref. [26], where a shell-model study of particle-hole nuclei around ^{100}Sn was performed. The value of $\epsilon_{h_{11/2}}$ has been increased of about 500 keV to reproduce the energy of the $11/2^-$ state at 980 keV in ^{111}Sn, which is predominantly of one-particle nature. The adopted SP energies are therefore the following (in MeV): $\epsilon_{g_{7/2}} = 0.0$, $\epsilon_{d_{5/2}} = 0.01$, $\epsilon_{s_{1/2}} = 2.2$, $\epsilon_{d_{3/2}} = 2.3$, and $\epsilon_{h_{11/2}} = 3.25$.

In the next section we present and compare with experiment the excitation energies we have obtained from a calculation performed by using the ANTOINE shell-model code [27]. In Sec. III B the calculated cross-section angular distributions for some states of ^{110}Sn are reported. They have been derived from a microscopic DWBA calculation and the needed two-nucleon transfer amplitudes have been computed within the framework of the seniority scheme by truncating the model space to states with seniority less than or equal to 4. In practice, the wave function for the ^{112}Sn ground state as well as those of the ^{110}Sn, including components with $v \leqslant 4$, are those resulting from a calculation based on the chain-calculation method described in Refs. [19,28]. We resorted to this approach because the two-nucleon transfer amplitudes are not provided by the ANTOINE code available to us [29].

In Fig. 6 the positive-parity spectrum of ^{110}Sn established in the present experiment is compared with the calculated one. All the theoretical states with $J^\pi = 0^+, 2^+, 4^+$, and 6^+ and excitation energy up to about 4.7 MeV are included. It is worth noting that, as it was the case for our previous results on ^{114}Sn [1] and light tin isotopes [30], the energy of the first 2^+ state is overestimated by our calculation. In fact, it is predicted at about 500 keV above the experimental one.

We have also found, as is the case for ^{114}Sn [1], that the observed excited 0^+ states are not well reproduced by the theory. We see that four excited 0^+ states have been experimentally identified with the highest-lying level at 3.183 MeV. In the same energy interval only three states are predicted by the theory, whereas other three states have an excitation energy between 3.8 and 4.5 MeV. When the observed states are associated with the four lowest calculated ones, a good agreement between the experimental and theoretical energies is obtained only for the first excited state. For the other three states the discrepancy ranges from 500 to 600 keV.

Let us now turn our attention to the $2^+, 4^+$, and 6^+ states. In the present experiment seven 2^+ levels have been populated above the first excited one and the same number is predicted by the theory in the energy interval 2.5–4.7 MeV. We may try to establish a one-to-one correspondence between the observed and calculated levels. It turns out that all the corresponding energies differ by less than 300 keV, exceeding this value only for the two highest-lying levels. The observed level density is well reproduced also for the 4^+ and 6^+ states. In fact, only one more 4^+ state is predicted by the theory with respect to the seven observed levels. It is worth noting that each of the six lowest-lying 4^+ levels can be identified with a state predicted by the theory, the discrepancies in the excitation energy ranging from few tens of keV to 300 keV. As for the seventh level at 4.317 MeV, it

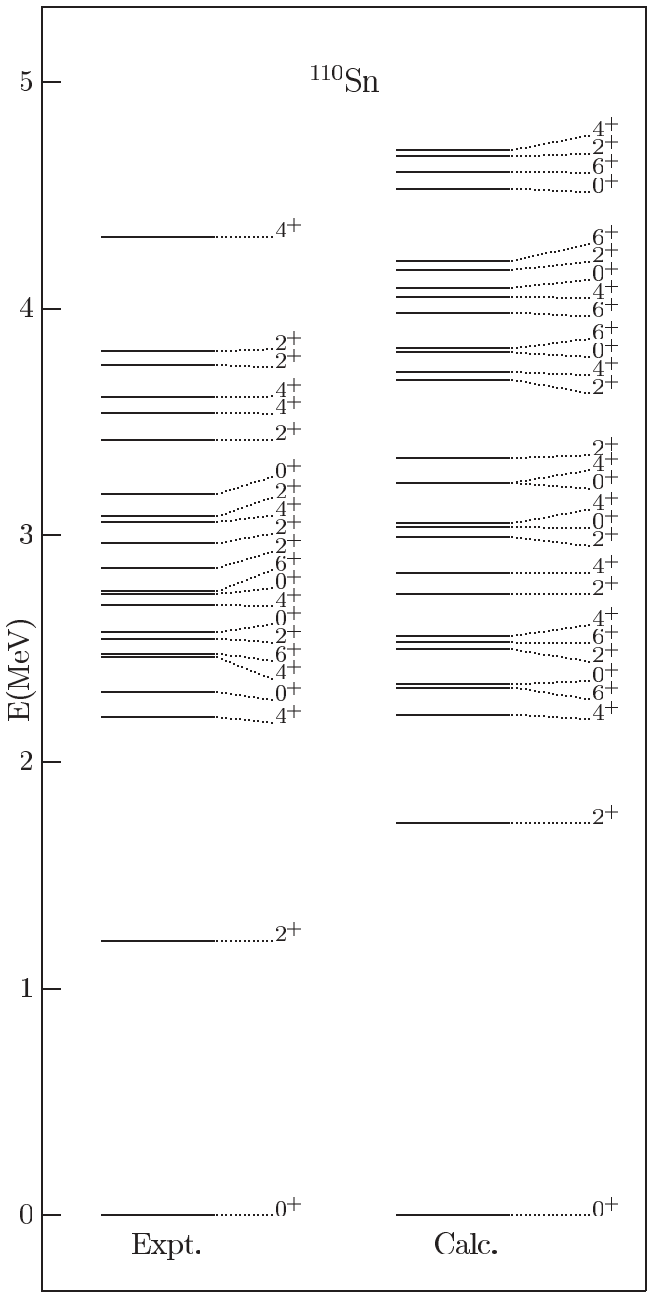

FIG. 6. Experimental and calculated positive-parity states in ^{110}Sn.

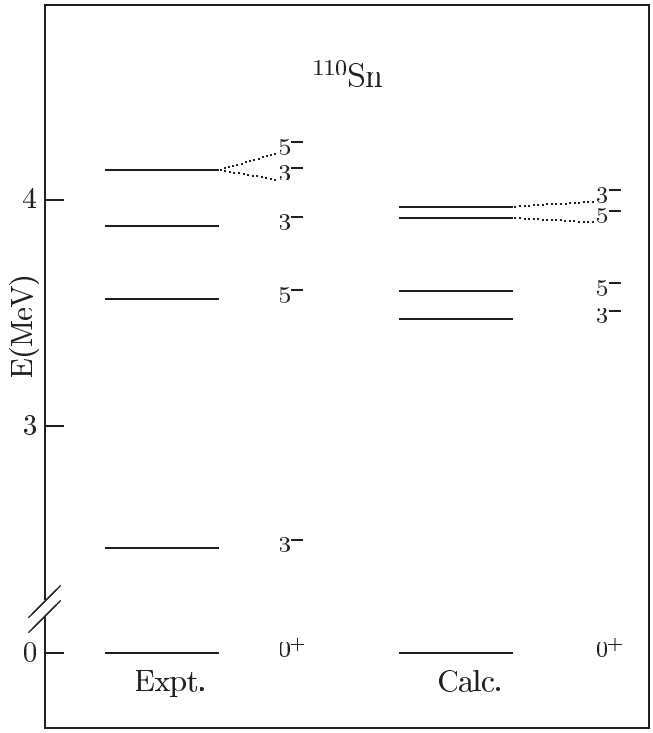

FIG. 7. Experimental and calculated negative-parity states in ^{110}Sn.

may be associated with either the 4_7^+ or the 4_8^+ calculated state, lying at 4.05 and 4.70 MeV, respectively. Finally, we see that the calculated energies of the two lowest 6^+ states are in good agreement with the values of the two observed 6^+ levels. It is worth noting that above 2.5 MeV our calculation predicts four more 6^+ states, which have not been found in the present experiment.

The negative-parity states observed in the present experiment are shown in Fig. 7, where we also report the calculated 3^- and 5^- states up to 4.3 MeV. We see that a correspondence between the experimental and theoretical 3^- states cannot be established without ambiguity. First, we note that only two 3^- states are predicted up to 4.3 MeV, the third calculated 3^- being at about 5 MeV excitation energy. If the observed levels are identified with the lowest calculated ones, it turns out that only the energy of the second state is well reproduced by the theory, whereas the positions of the first and third states are overestimated by more than 800 keV. However, we cannot exclude that the first 3^- state at 2.46 MeV has no theoretical counterpart, because its description requires a substantial contribution from particle-hole excitations that are outside our model space. This latter hypothesis implies that the second and third observed 3^- state may be associated with the two lowest calculated ones, the energies differing in this case by about 400 and 150 keV, respectively. As for the two 5^- experimental states, they can be identified with the two lowest calculated ones, the difference between experimental and theoretical energy being less than 260 keV for both states.

B. Form factors and comparison with the experimental angular distributions

In Sec. II B, a cluster DWBA analysis was used to provide (p, t) angular distributions to guide the attribution of L values to individual final states. This analysis included geometrical and physical features of the process, such as absorption, barrier penetration, and angular momentum transfer. The shape of the angular distribution was calculated for each final state, and a multiplicative factor was chosen to produce the best visual fit to the measured data points. However, no attempt was made to calculate the relative cross sections in Figs. 2–5 for the different final states. To do this, we need wave functions for the ^{112}Sn ground state and for each ^{110}Sn final state. We also

need a more detailed theory of the reaction process, specifying whether it occurs in a single pickup of two neutrons, or two successive one-neutron pickups. In this section, we will use the wave functions generated in the shell-model calculation described in Sec. III A, and the simplest microscopic transfer theory, which assumes that the reaction occurs in one step via an interaction which is a delta function of the vector between the proton and the two transferred neutrons. The details of this theory have been presented in many places [31,32].

The main link between the reaction amplitude and the microscopic structures of the target and residual states is the *spectroscopic amplitude* $S^J_{n_1,\ell_1,j_1;n_2,\ell_2,j_2}$. For a situation such as ours, in which the (p,t) target state has angular momentum zero, this is defined by the matrix element

$$S^J_{n_1,\ell_1,j_1;n_2,\ell_2,j_2} \equiv \left\langle \Psi^0_0(\text{target}) \left| \left[\frac{\left[a^+_{n_1,\ell_1,j_1} a^+_{n_2,\ell_2,j_2}\right]^J}{\left(1+\delta_{n_1,n_2}\delta_{\ell_1,\ell_2}\delta_{j_1,j_2}\right)} \times \Psi^J(\text{residual}) \right]^0_0 \right\rangle, \tag{1}$$

where the square brackets signify vector coupling and $a^+_{n,\ell,j,m}$ creates a neutron in the single-particle shell-model state $\psi^{n,\ell,j}_m$. The spectroscopic amplitudes can be calculated once the target and residual wave functions, Ψ^0_0(target) and Ψ^J_M(residual), are known. The wave function of the transferred neutrons is then

$$\sum_{n_1,\ell_1,j_1;n_2,\ell_2,j_2} S^J_{n_1,\ell_1,j_1;n_2,\ell_2,j_2} \frac{[\psi^{n_1,\ell_1,j_1}(\mathbf{r}_1,\sigma_1)\psi^{n_2,\ell_2,j_2}(\mathbf{r}_2,\sigma_2)]^J_M - [\psi^{n_1,\ell_1,j_1}(\mathbf{r}_2,\sigma_2)\psi^{n_2,\ell_2,j_2}(\mathbf{r}_1,\sigma_1)]^J_M}{2(1+\delta_{n_1,n_2}\delta_{\ell_1,\ell_2}\delta_{j_1,j_2})}. \tag{2}$$

The coherence of the components associated with the different transferred configurations is characteristic of direct theories of multinucleon transfer. It is then required to project from this wave function the part in which the two neutrons have relative orbital angular momentum zero and total spin zero. The result, which is a function of the center-of-mass coordinate of the two neutrons, serves as the form factor of a DWBA code. The calculated angular distributions shown below used the code TWOFNR ([15]). One consequence of this theory is that only natural-parity residual states can be reached if the target state is 0^+.

Because of the physically small size of the triton, and the fact that the total neutron spin of the triton is zero, the (p,t) reaction is strong when the transfer wave function (2) represents a strongly correlated neutron pair, such as is produced by a neutron pairing force. This implies that a target ground state will be most strongly connected to the low-lying states of the residual nucleus. These states are low in energy because pairing correlations are strong.

The optical parameters used for the proton and triton continuum wave functions are given in Table III. The parameters of the well in which the neutron bound-state wave functions, $\psi^{n,\ell,j}_m$, were calculated are $r_r = 0.65$ fm, $a_r = 0.65$ fm, $V_{so} = 6.0$ MeV. The depth of the central well was adjusted so that the binding energy of each of the neutrons was half the two-neutron separation energy for the ^{112}Sn ground state and each ^{110}Sn residual state.

The zero-range one-step DWBA approach used here should give an accurate description of the shapes of the angular distributions, and the relative cross sections for different residual states of different angular momenta, but it is unable to calculate their absolute cross sections. Therefore a *single* multiplicative factor must be chosen before the DWBA output can be compared to experimental data. This is in contrast to the analysis presented in Sec. II B, where a *different* multiplicative factor was used for each state. We have chosen this single multiplicative factor to produce the best visual fit with the ground-state cross section. The result is shown in Fig. 8, where we have also included predictions and data for the lowest 2^+ and 4^+ transitions. It is seen that our shell-model wave functions, and the simple one-step zero-range microscopic analysis, yield an excellent account of the population of the lowest three states in our observed spectrum.

There are other cases, however, where these assumptions yield predictions that are inconsistent with our measurements. For example, the (p,t) cross section for excitation of the lowest 6^+ state, and the second 0^+ and 2^+ states are overpredicted by the theory when the same normalization as in Fig. 8 is used. The calculated 6^+ angular distribution has to be scaled down by a factor 4, and the corresponding factors for the

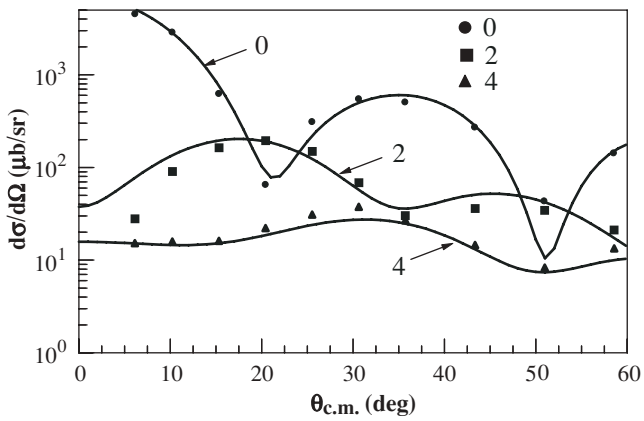

FIG. 8. Comparison of microscopic DWBA calculations and experimental differential cross sections for the lowest 0^+, 2^+, and 4^+ states of ^{110}Sn. A single normalization factor is used for all three states.

second 0^+ and 2^+ levels are 10 and 5, respectively. Let us now investigate the possible origin of this discrepancy for the 0^+ state ($E = 2.309$ MeV). We write the expression for the differential cross section of the $i^{\text{th}}0^+$ state in the form

$$\frac{d\sigma^i}{d\Omega}(\theta) = \left| \sum_{n\ell j} S^i_{n\ell j} f_{n\ell j}(\theta) \right|^2 . \tag{3}$$

Here $S^i_{n\ell j}$ is the spectroscopic amplitude, calculated from our shell-model wave functions, for the transfer of the zero-coupled pair $[\psi^{n\ell j}(\mathbf{r}_1, \sigma_1)\psi^{n\ell j}(\mathbf{r}_2, \sigma_2)]^0_0$ in the transition to the $i^{\text{th}}0^+$ state of ^{110}Sn. The associated reaction amplitude $f_{n\ell j}(\theta)$ is calculated by the DWBA reaction code. It is implied in Eq. (3) that $f_{n\ell j}(\theta)$ is the same for the ground and excited 0^+ states. This is not strictly true, because the Q value difference means that barrier penetration effects for the outgoing triton will be somewhat different, but with a 26-MeV incident proton, the difference is small.

Because the reaction is mostly confined to the nuclear surface, the angular shapes of the $f_{n\ell j}(\theta)$ are approximately independent of $n\ell j$, for a given set of optical parameters so that we can write, approximately,

$$f_{n\ell j}(\theta) \sim C_{n\ell j} f(\theta). \tag{4}$$

Then Eq. (3) becomes

$$\frac{d\sigma^i}{d\Omega}(\theta) \sim \left| \sum_{n,\ell,j} S^i_{n\ell j} C_{n\ell j} \right|^2 |f(\theta)|^2. \tag{5}$$

Thus to compare the predicted cross sections for the population of the ground and 2.309-MeV 0^+ states, we need only compare $|\sum_{n,\ell,j} S^i_{n\ell j} C_{n\ell j}|^2$ for $i = 0$ and 2.309.

As mentioned above, the $S^i_{n\ell j}$ are taken from our shell-model calculation, whereas the $C_{n\ell j}$ can be obtained by running the DWBA code for a pure $n\ell j$ configuration, in which case the calculated differential cross section (whose angular dependence is nearly the same for all $n\ell j$), will be proportional to $(C_{n\ell j})^2$. With the time-reversal phases used by the code TWOFNR, all the $C_{n\ell j}$ will have the same sign. In this way, we have constructed Table IV. The relative values of the $C_{n\ell j}$ in Table IV are meaningful, but they contain an overall arbitrary multiplicative factor (as do all our DWBA cross sections).

$C_{1d5/2}$ in Table IV is larger than $C_{1d3/2}$ mainly because $[\psi^{1d5/2}(1)\psi^{1d5/2}(2)]^0_0$ has a larger $L = S = 0$ component than $[\psi^{1d3/2}(1)\psi^{1d3/2}(2)]^0_0$. $C_{0g7/2}$ and $C_{0h11/2}$ are relatively small because their high single-particle orbital angular momenta imply high relative momenta of the two neutrons in the surface, which produces a poor match with the relative momenta of the neutrons in the triton. A similar phenomenon occurs in the f-p shell, where $[\psi^{1p3/2}(1)\psi^{1p3/2}(2)]^0_0$ transfer is stronger than $[\psi^{0f7/2}(1)\psi^{0f7/2}(2)]^0_0$ transfer [33].

TABLE IV. Spectroscopic and reaction amplitudes for the two lowest 0^+ states of ^{110}Sn.

$n\ell j$	$C_{n\ell j}$	$S^0_{n\ell j}$	$C_{n\ell j}S^0_{n\ell j}$	$S^{2.309}_{n\ell j}$	$C_{n\ell j}S^{2.309}_{n\ell j}$
$0g_{7/2}$	.483	−1.1073	−.535	−.3186	−.154
$1d_{5/2}$	2.91	−.7556	−2.199	.6783	1.974
$1d_{3/2}$	1.96	−.4825	−.946	.0400	.078
$2s_{1/2}$	2.87	−.3663	−1.051	−.0015	−.004
$0h_{11/2}$	.672	−.6647	−.447	.0289	.019

The fourth column of Table IV gives the contribution of each orbital to the ground-state transition. The main characteristic of the ground-state transition (if pairing effects are important) is that all contributions have the same sign, so we get constructive interference. This leads to

$$\sum_{n\ell j} C_{n\ell j} S^0_{n\ell j} = -5.178 \qquad \left(\sum_{n\ell j} C_{n\ell j} S^0_{n\ell j} \right)^2 = 26.81.$$

For the $E = 2.309$ MeV contribution, the contributions do not have the same sign. We get

$$\sum_{n\ell j} C_{n\ell j} S^{2.309}_{n\ell j} = 1.913 \qquad \left(\sum_{n\ell j} C_{n\ell j} S^{2.309}_{n\ell j} \right)^2 = 3.66.$$

This approximate calculation implies a ratio of $26.81/3.66 = 7.3$ for the cross sections of the two lowest 0^+ states. A more accurate calculation, including Q-value effects, yields a ratio of about 10. However, the data of Table II show that we have measured the ratio to be about $1309/12 = 110$. Thus shell-model plus DWBA strongly overpredicts the population of the $E = 2.309$ MeV state relative to the ground state.

It is clear from the last column of Table IV that we cannot resolve this discrepancy by making small changes in the spectroscopic amplitudes for the $E = 2.309$ MeV state, so as to achieve enough destructive interference to reduce the calculated cross section by a factor of 11. The $\sum_{n\ell j} C_{n\ell j} S^{2.309}_{n\ell j}$ sum is dominated by the single term arising from $[\psi^{1d5/2}(1)\psi^{1d5/2}(2)]^0_0$ transfer, and so small changes in the other spectroscopic amplitudes can have little effect.

It may be that this comparison implies that $E = 2.309$ MeV state cannot be understood in terms of neutron degrees of freedom alone. All the nuclear wave functions considered so far confined the 50 protons to filled shells, up to and including $0g_{9/2}$. These may give a good description of the ^{112}Sn ground state, and the lowest 0^+, 2^+, and 4^+ states of ^{110}Sn, but it is possible that the $E = 2.309$ MeV 0^+ state contains two-particle, two-hole proton components. In fact, there is evidence [34] that there is a two-particle, two-hole proton component in a 0^+ state in ^{112}Sn at a similar excitation energy. Obviously, if the ^{112}Sn ground state has filled proton shells, a one-step two-neutron transfer process such as a (p, t) reaction could only connect with components of ^{110}Sn wave functions with filled protons shells. It could not connect to components of ^{110}Sn states with particle-hole proton excitations. Thus, the transition to a real ^{110}Sn state can be expected to be weaker than a transition to a model ^{110}Sn state in which there are no particle-hole proton excitations. If this is the explanation of the excited 0^+ discrepancy, it must be that the amplitude of the particle-hole component of the $E = 2.309$ MeV state is more than three times as great as the amplitude of the component with filled proton shells. Nevertheless, our calculation of the energy of this state was correct to within only 60 keV. This is likely to be related to our two-body effective interaction that,

as discussed in Sec. III A, includes particle-hole excitations through second-order diagrams in $V_{\text{low-k}}$. We believe that this example demonstrates that (p, t) cross-section measurements can provide sensitive tests of nuclear model predictions, in some cases more sensitive than comparison of measured and calculated excitation energies.

IV. SUMMARY

The ^{112}Sn$(p, t)^{110}$Sn reaction has been studied in a high-resolution experiment carried out at an incident proton energy of 26 MeV. Cross-section angular distributions for 27 transitions to levels of ^{110}Sn up to an excitation energy of ∼4.3 MeV have been measured. The spin and parity for all the observed levels have been assigned by a DWBA analysis, assuming a semimicroscopic dineutron cluster pickup mechanism. The calculations have been performed in finite-range approximation.

Nine levels have been observed for the first time and identified in J^π. With respect to the adopted levels, 10 levels have been confirmed and four ambiguities removed. Two unresolved doublets have been observed, giving one confirmation, one removed ambiguity and two new assignments.

For a better understanding of the ^{110}Sn nucleus, the present (p, t) experimental data have been supplemented with zero-range one-step DWBA microscopic calculations of cross-section angular distributions for the ground state and some excited states of ^{110}Sn. These microscopic calculations have been performed using two-neutron spectroscopic amplitudes obtained from a shell-model study of the 12- and 10-neutron systems outside the $N = 50$ neutron major shell, for the ^{112}Sn and ^{110}Sn nuclei, respectively. The shell-model calculations have been carried out within the framework of the seniority scheme, using a realistic effective interaction derived from the CD-Bonn nucleon-nucleon potential. The model space has been truncated to states with seniority less than or equal to 4 to reduce the numerical work required by a complete basis diagonalization. The shell-model wave functions used and the simple one-step zero-range microscopic analysis yield an excellent account of the population of the lowest three states of the observed ^{110}Sn spectrum. On the contrary as we move to higher excited states, 0_2^+, 2_2^+, 6_1^+, the theory overpredicts the (p, t) cross sections, compared to the yrast 0^+, 2^+, and 4^+ levels. In particular, the case of the 0_2^+ state is discussed in detail.

A full shell-model study of both positive- and negative-parity spectra of ^{110}Sn has been also performed. As regard the positive-parity states, the 0^+ states are not well reproduced by the theory. Regarding the 2^+ states, a one-to-one correspondence between the observed and calculated levels may be established and the observed level density is well reproduced also for the 4^+ and 6^+ states.

As regards the negative-parity states, whereas a correspondence between the experimental and theoretical 3^- states cannot be established without ambiguity, the two 5^- experimental states can be identified with the two lowest calculated ones.

[1] P. Guazzoni, L. Zetta, A. Covello, A. Gargano, G. Graw, R. Hertenberger, H.-F. Wirth, and M. Jaskóla, Phys. Rev. C **69**, 024619 (2004).
[2] R. Oxorn, A. J. Houdayer, and S. K. Mark, Z. Phys. A **279**, 289 (1976).
[3] A. Van Poelgest, J. Bron, W. H. A. Hesselink, K. Allaart, J. J. A. Zalmstra, M. J. Uitzinger, and H. Verheul, Nucl. Phys. **A346**, 70 (1980).
[4] W. Andrejtscheff, L. K. Kostov, P. Petkov, Y. Sy. Savane, Ch. Stoyanov, P. Von Brentano, J. Eberth, R. Reinhardt, and K. O. Zell, Nucl. Phys. **A505**, 397 (1989).
[5] D. A. Viggars, H. W. Taylor, B. Singh, and J. C. Waddington, Phys. Rev. C **36**, 1006 (1987).
[6] H. Harada, T. Marukami, K. Yoshida, J. Kasagi, T. Inamura, and T. Kubo, Phys. Lett. **B207**, 17 (1988).
[7] D. G. Fleming, M. Blann, H. W. Fulbright, and J. A. Robbins, Nucl. Phys. **A157**, 1 (1970).
[8] P. J. Blankert, Ph.D. thesis, Vrije Universiteit Amsterdam (1979).
[9] R. Machleidt, Phys. Rev. C **63**, 024001 (2001).
[10] P. Guazzoni, L. Zetta, A. Covello, A. Gargano, G. Graw, R. Hertenberger, H.-F. Wirth, B. F. Bayman, and M. Jaskóła, in *Key Topics in Nuclear Structure*, Proceedings of the 8th International Spring Seminar on Nuclear Physics, Paestum, 2004, edited by A. Covello (World Scientific, Singapore, 2005), p. 275.
[11] M. Loeffer, H. J. Scheere, and A. Vonach, Nucl. Instrum. Methods **111**, 1 (1973).
[12] E. Zanotti, M. Bisenberger, R. Hertenberger, H. Kader, and G. Graw, Nucl. Instrum. Methods Phys. Res. A **310**, 706 (1991).
[13] J. R. Comfort, ANL Physics Division, Report No. PHY 19708, Argonne 1970.
[14] D. De Frenne and E. Jacobs, Nucl. Data Sheets **89**, 481 (2000).
[15] M. Igarashi, computer code TWOFNR (1977), unpublished.
[16] F. G. Perey, Phys. Rev. **131**, 745 (1963).
[17] R. L. Varner, W. J. Thompson, T. L. Mc Abee, E. J. Ludwig, and T. B. Clegg, Phys. Rep. **201**, 57 (1991).
[18] R. A. Hardekopf, R. F. Haglund Jr., G. G. Ohlsen, W. J. Thompson, and L. R. Veeser, Phys. Rev. C **21**, 906 (1980).
[19] P. Guazzoni, M. Jaskóla, L. Zetta, A. Covello, A. Gargano, Y. Eisermann, G. Graw, R. Hertenberger, A. Metz, F. Nuoffer, and G. Staudt, Phys. Rev. C **60**, 054603 (1999).
[20] G. Cata-Danil, P. Guazzoni, M. Jaskóla, L. Zetta, G. Graw, R. Hertenberger, D. Hofer, P. Schiemenz, B. Valnion, E. Zanotti-Mueller, U. Atzrott, F. Hoyler, F. Nuoffer, and G. Staudt, J. Phys. G **22**, 107 (1996).
[21] P. Guazzoni, M. Jaskóla, V. Yu. Ponomarev, L. Zetta, G. Graw, R. Hertenberger, and G. Staudt, Phys. Rev. C **62**, 054312 (2000).
[22] S. Bogner, T. T. S. Kuo, L. Coraggio, A. Covello, and N. Itaco, Phys. Rev. C **65**, 051301(R) (2002).
[23] T. T. S. Kuo, S. Y. Lee, and K. F. Ratcliff, Nucl. Phys. **A176**, 65 (1971).
[24] K. Suzuki and S. Y. Lee, Prog. Theor. Phys. **64**, 2091 (1980).
[25] M. F. Jiang, R. Machleidt, D. B. Stout, and T. T. S. Kuo, Phys. Rev. C **46**, 910 (1992).
[26] L. Coraggio, A. Covello, A. Gargano, and N. Itaco, Phys. Rev. C **70**, 034310 (2004).
[27] E. Caurier and F. Nowacki, Acta Phys. Pol. B **30**, 705 (1999).

[28] A. Covello, F. Andreozzi, L. Coraggio, A. Gargano, and A. Porrino, in *Contemporary Nuclear Shell Models*, Lecture Notes in Physics Vol. 482 (Springer-Verlag, Berlin, 1997).
[29] Our version was downloaded from the URL: http://sbgat194.in2p3.fr/~theory/antoine/menu.html.
[30] F. Andreozzi, L. Coraggio, A. Covello, A. Gargano, T. T. S. Kuo, Z. B. Li, and A. Porrino, Phys. Rev. C **54**, 1636 (1996).
[31] B. F. Bayman and A. Kallio, Phys. Rev. **156**, 1126 (1967).
[32] D. N. Mihailidis, N. M. Hintz, A. Sethi, and E. J. Stephenson, Phys. Rev. C **64**, 054608 (2001).
[33] B. F. Bayman and N. M. Hintz, Phys. Rev. **172**, 1113 (1968).
[34] G. Bonsignori, M. Savoia, K. Allaart, A. van Egmond, G. Te Velde, Nucl. Phys. **A432**, 389 (1985).